

STELLAR BAR EVOLUTION IN CUSPY AND FLAT-CORED TRIAXIAL CDM HALOS

INGO BERENTZEN AND ISAAC SHLOSMAN

Department of Physics and Astronomy, University of Kentucky, Lexington, KY 40506-0055, USA
email: iberent@pa.uky.edu, shlosman@pa.uky.edu

AND

SHARDHA JOGEE

Department of Astronomy, University of Texas at Austin, 1 University Station C1400, Austin, TX 78712, USA
email: sj@astro.as.utexas.edu

To be published by the Astrophysical Journal

ABSTRACT

We analyze the formation and evolution of stellar bars in galactic disks embedded in *mildly* triaxial cold dark matter (CDM) halos that have density distributions ranging from large flat cores to cuspy profiles. We have applied tailored numerical simulations of analytical and live halos which include the feedback from disk/bar system onto the halo in order to test and extend earlier work by El-Zant & Shlosman (2002). The latter employed the method of Liapunov exponents to analyze the fate of bars in analytical asymmetric halos. We find the following: (1) The bar growth is very similar in all *rigid* axisymmetric and triaxial halos. (2) Bars in live models experience vertical buckling instability and the formation of a pseudo-bulge with a boxy/peanut shape, while bars in rigid halos do not buckle. (3) In *live* axisymmetric halos, the bar strength varies by a factor of $\lesssim 2$, in growth or decay, during the secular evolution following the buckling. The bar pattern speed evolution (i.e., deceleration) anticorrelates with the halo core size. In such halos, the bar strength is larger for smaller disk-to-halo mass ratios D/H within disk radii, the bar size correlates with the halo core sizes, and the bar pattern speeds correlate with the halo central mass concentration. In contrast, bars embedded in *live* triaxial halos have a starkly different fate: they dissolve on a timescale of $\sim 1.5 - 5$ Gyr due to the onset of chaos over continuous zones, sometimes leaving behind a weak oval distortion. The onset of chaos is related to the halo triaxiality, the fast rotating bar and the halo cuspidity. Before the bar dissolves, the region outside it develops strong spiral structures, especially in the live triaxial halos. (4) More angular momentum is absorbed (fractionally) by the triaxial halos as compared to the axisymmetric models. The disk-halo angular momentum exchange is mediated by the lower resonances in the latter models. (5) Cuspy halos are more susceptible than flat-core halos to having their prolateness washed out by the action of the bar. The subsequent evolution is then similar to the case of a cuspy axisymmetric halos. We analyze the above results on disk and bar evolution in terms of the stability of trajectories and development of chaos in the system. We set important constraints on the triaxiality of DM halos by comparing our predictions to recent observational results on the properties of bars out to intermediate redshifts $z \sim 1$.

Subject headings: galaxies: evolution – galaxies: formation – galaxies: halos – galaxies: kinematics and dynamics – galaxies: structure – cosmology: dark matter

1. INTRODUCTION

Stellar bars are recognized as the single most important *internal* factor which drives the evolution of disk galaxies both dynamically and secularly, modifying their morphology in this process. Modern understanding of the bar growth is based on the efficiency of angular momentum exchange between the (bar-forming) inner disk and the surrounding dark matter halo, outer disk, bulge, and, to a certain degree, with the immediate galactic environment (Athanasoula 2003). A number of yet to be identified and investigated intricacies can affect the efficiency of this process.

In this work we attempt to analyze the formation and evolution of stellar bars embedded in fully grown disks in the presence of *triaxial*¹ halos with various radial density profiles, from cuspy to flat-core models. We study both analytical (i.e., rigid) and live triaxial halos and compare our results with the evolution of the bars in ax-

isymmetric ones. Corollaries for disk evolution, such as the back-reaction of disks and bars on the halo shapes, are investigated as well. This effect has broad implications for the cosmological evolution of galaxies. Additional evolutionary effects on the 3-D structure of stellar bars embedded in such halos will be addressed elsewhere.

The evolution of bars is expected to be substantially altered if the surrounding halos are even mildly non-axisymmetric (El-Zant & Shlosman 2002, hereafter ES02). However, this effect in a live disk-halo system was not verified so far. Competing gravitational torques from a bar and a halo acting on the main families of planar and 3-D periodic orbits can destabilize them and dramatically reduce their ability to trap neighboring trajectories, thus inducing chaos and dissolving otherwise stable structural features in disk galaxies. The full extent of these non-linear effects is not yet clear, but one can expect them to speed up secular changes in the collisionless components and to facilitate the angular momentum loss in the gaseous one. Although triaxial shapes of dark

¹ We also use the term ‘asymmetric’ concurrently with ‘triaxial’

matter halos appear inherent in the cosmological numerical simulations (e.g., Barnes & Efstathiou 1987; Frenk et al. 1988; Dubinski & Carlberg 1991; Warren et al. 1992; Cole & Lacey 1996), relatively little attention has been paid so far to this issue when building self-consistent galactic models.

Observational constraints on the *shapes* of galactic halos coming from gas kinematics in disk galaxies (e.g., Sparke 1986; Sackett 1999; Andersen et al. 2001; Merrifield 2002; Dekel & Shlosman 1983) and their polar rings (Sackett et al. 1994; Sackett & Pogge 1995), gravitational lensing (Kochanek 1995; Oguri et al. 2003; Hoekstra, Yee & Gladders 2004) and X-ray gas in ellipticals (Buote & Canizares 1994, 1996; Buote et al. 2002) remain inconclusive.

Nevertheless, some clues exist. Residual *potential* axial ratios (both flatness and prolateness²) of about 0.9 in Cold Dark Matter (hereafter CDM) halos are plausible, even in *present* day galaxies (e.g., Kuijken & Tremaine 1994 [for the Milky Way]; Rix & Zaritsky 1995; Helmi 2004). Another evidence for triaxiality of the DM halo is provided by the X-ray isophote position angle twist observed by *Chandra* in NGC 720 (but not in stellar isophotes!) (Buote et al. 2002). A nearly prolate DM halo, with $T \sim 0.985$ (and $b/a \sim 0.791$, $c/a \sim 0.787$) has been inferred for the elliptical galaxy NGC 5128 from a kinematic study of planetary nebula system (Peng et al. 2004). We conjecture, therefore, that while some individual halo shapes are compatible with being mildly prolate even at the present time, the statistical significance of this effect is not clear, and it is not clear whether disk galaxies differ in this respect from ellipticals. Overall, the prolateness of *contemporary* halos appears to be insignificant.

The main motivation behind this work is that theoretically a galactic halo is expected to acquire its triaxial shape during its initial collapse and to support this shape during the ongoing process of a hierarchical merging. The degree of triaxiality³ will depend on the merging history, specifically on the relative angular momenta of the merger precursors and interaction frequency — which is difficult to quantify.

Numerical simulations indicate that at very high redshifts, at the epoch of galaxy formation, the halos can be significantly triaxial. Detailed properties of individual numerical halos, such as triaxial shapes and radial density structure, can be extracted from the models and directly confronted by their observational counterparts. Flatness and prolateness in the models appear to increase with the halo mass, being somewhat milder in the Λ CDM than CDM cosmology (e.g., for a recent review Bullock 2002). This triaxiality seems to be marginally higher in the outer halo parts, independently of the halo mass and of the ratio of rotational-to-dispersion velocity, indicating that the halos are supported by anisotropic velocity dispersions.

The high halo triaxiality that may be present at the epoch of early galaxy formation can be substantially di-

luted by the present-day. For instance, the addition of spherical and/or axisymmetric baryonic components to the system (e.g., during the formation and development of a galactic disk) can wash out the halo triaxiality, still keeping it non-negligible (Dubinski 1994; Kazantzidis et al. 2004).

From an observational standpoint it appears that *profiles* of the DM halos in fully formed galaxies tend to have nearly constant density cores (Flores & Primack 1994; Moore 1994; Burkert 1995; Kravtsov et al. 1998; Borriello & Salucci 2001; de Blok & Bosma 2002; Gentile et al. 2004; etc.). A similar effect has been recently observed in galactic clusters (Sand et al. 2002). At the same time, dissipationless CDM simulations of galactic halos agree with a universal density profile $\propto r^{-\alpha}$, where $\alpha = 1 - 1.5$ (e.g., Dubinski & Carlberg 1991; Warren et al. 1992; Crone et al. 1994; Cole & Lacey 1996; Tormen et al. 1997; Huss et al. 1999; Fukushige & Makino 1997; Moore et al. 1999; Klypin et al. 2000; Jing & Suto 2002; Power et al. 2003). (Note, Jing & Suto (2000) claim that the profiles are not universal.) Navarro, Frenk & White (1996, hereafter NFW) have found a fitting formula for the density profile of DM halos, for a wide range of cosmological models, in which the inner profile diverges as r^{-1} , while the outer profile drops as r^{-3} . It has been also demonstrated theoretically that a cuspy density profile arises inherently from the cold gravitational collapse in an expanding universe (Lokas & Hoffman 2000). The CDM model, therefore, predicts that the inner density profile of galactic scale DM halos is characterized by a density cusp while observations of the dynamics of the central regions of galaxies imply a core-halo structure of the DM. Another disagreement with observations is the so-called angular momentum catastrophe — the N -body and gas dynamical simulations consistently result in too small galactic disks due to the overall lack of angular momentum necessary to reproduce the observed disk sizes (e.g., Burkert & D’Onglia 2004).

This controversy between observations of DM cores and density cusps in numerical models is not a fundamental one and can be resolved within the general context of CDM cosmology. Within the conventional physics framework, interactions with the dissipative and clumpy baryonic component, such as dynamical friction, during the initial stages of collapse can level off the central density cusps (which have been shown to be thermodynamically improbable) and produce harmonic cores in DM halos (El-Zant, Shlosman & Hoffman 2001). Even though this may affect the isodensity contours, making them rounder, it need not symmetrize the isopotentials; these can remain asymmetric if triaxiality is not affected beyond some radius (for example, a uniform bar has a non-axisymmetric force contribution inside its density figure). More generally, this process was shown to replace the DM cusps with baryonic cusps (El-Zant et al. 2004). Furthermore, asymmetric and flat core halos can have interesting implications for the disk growth and correlate the properties of the central supermassive black holes with those of galactic bulges and halos themselves (El-Zant et al. 2003). Alternatively, the central density cusps have been proposed to dissolve by the action of galactic bars (Weinberg & Katz 2002; but see McMillan & Dehnen 2005).

A number of approaches can be taken in order to

² We define the halo flatness as $f = 1 - c/a$ and its prolateness (i.e., equatorial ellipticity) as $e_H = 1 - b/a$

³ The triaxiality is defined here as $T = [1 - (b/a)^2]/[1 - (c/a)^2]$, where c/a is halo’s polar-to-longest equatorial axis ratio and b/a – equatorial axis ratio. $T = 1$ corresponds to a prolate halo, while $T = 0$ to an oblate one

construct triaxial halos and elliptical galaxies (e.g., Aarseth & Binney 1974; Merritt & Valluri 1996; Holley-Bockelmann et al. 2001; Moore et al. 2004) and to study the bar dynamics within triaxial halos. Ireta & Hozumi (2000) have used analytical density distributions for two highly prolate halos with (equatorial) axial ratios of 0.6 and 0.75 and a very steep density distribution outside the core. Here we choose to construct stable triaxial models with a subsequent introduction of axisymmetric collisionless disks which are then released and their time evolution is observed. In our initial conditions we tend to follow ES02, who studied systematically the stability of stellar bars in *analytical* halos of different triaxiality and central concentration by means of Liapunov exponents. While in ES02 approach the feedback from disk/bar system onto the halo is naturally ignored, our models presented here fully account for it.

In ES02, mildly triaxial shapes have been used, with the gravitational potential axial ratios in the equatorial plane, b/a , between 0.9 and 1.0, and $c/a = 0.8$, where c is the halo polar axis. A clear trend has been found, in the sense of models becoming intrinsically chaotic with growing triaxiality and central concentration. For small halo (flat) core sizes, $\sim 0.5 - 2$ kpc, and potential axis ratios of 0.9 – 0.95 most of the trajectories integrated appeared chaotic and had large Liapunov exponents. Importantly, trapping by neighboring stability islands is insignificant, because the distribution of values of Lyapunov exponents is very similar to the distribution of occupied configuration space volume. This means that stellar bars under these conditions would disintegrate on timescales of a few dynamical times, much shorter than the Hubble time, as chaotic trajectories quickly diffuse out of the bar’s configuration space. Even spherically-symmetrical models, with a small core size, showed a healthy fraction of chaotic trajectories, though connected regions of regular orbits aligned with the bar remained in this case and a self-consistent bar could be maintained.

What are the reasons for a dramatic increase in the fraction of chaotic orbits in the barred disks with the increase in central concentration (i.e., cuspsiness) and triaxiality in the halo models of ES02? First, in terms of invariants of motion, a stable 3-D figure must be built from trajectories which at least approximately conserve them. The chaos appears when the number of invariants of motion becomes smaller than the dimensionality of the system. While in the flat core systems, the potential can be approximated as quadratic (i.e., harmonic) and motions along the coordinates are independent of each other, in cuspy potentials these motions are coupled, which leads to the overall decrease in the number of invariants of motion and typically to a chaotic behavior. In other words, cuspy density distribution cause solutions for the Poisson equation to be far from quadratic, i.e., when the potential is expanded in power series, it will have a non-negligible contribution from terms beyond the quadratic one. These terms produce the coupling between different degrees of freedom in equations of motion which become highly non-linear. Such systems are prime candidates to excite chaotic motions when perturbed.

The second reason is related to the time-dependent character of the azimuthal force field comprised from the

fast rotating⁴ bar and a non- or slowly tumbling halo. In other words, the origin of chaos in this case lies in the comparable (in value) and competing forces from the bar and the asymmetric halo. (Note, that in a halo potential only, most of the orbits are regular, even in the triaxial case.)

This onset of chaos in the presence of a bar within even a mildly triaxial halo hints that such configurations are structurally unstable on dynamical timescales. Since numerical cosmological halos are both triaxial and centrally-concentrated, serious questions arise about the survival of large-scale stellar bars or of the halos’s triaxiality under these conditions. This issue defines the general thrust of our work.

This paper is structured as follows. In the next section we provide the initial conditions for numerical modeling. Sections 3 and 4 describe our results for analytical and live models, and section 5 is devoted to discussion and concluding remarks.

2. NUMERICAL MODELING

We have introduced the following dimensionless model units. The spatial distance unit is taken as $r = 10$ kpc, the mass unit is $M = 10^{11} M_{\odot}$ and the gravitational constant is chosen to be $G = 1$, which result in a time unit of $\tau = (r^3/GM)^{1/2} = 4.7 \times 10^7$ yrs, corresponding to the dynamical timescale, τ_{dyn} . In these units, the velocity is given in 208 km s^{-1} . The actual physical units are used when it is needed for clarity.

We have used version FTM-4.4 of N -body code (e.g., Heller & Shlosman 1994; Heller 1995) with $N = 6 - 9 \times 10^5$ particles and gravitational softening of 100 pc to simulate the collisionless disk and spheroidal galactic components (i.e., bulges and DM halos) in a large number of models. Our results appear to be reasonably independent of N . The gravitational forces have been computed using Dehnen’s (2002) `fa1cON` force solver, a tree code with mutual cell-cell interactions and complexity $O(N)$. It conserves momentum exactly and is about 10 times faster than optimally coded Barnes & Hut (1986) tree code.

To analyze the angular momentum redistribution in the models, we have applied the spectral analysis method described in Binney & Spergel (1982), in conjunction with our nonlinear orbit finding algorithm (e.g., Heller & Shlosman 1996). Athanassoula (2002) has shown that the angular momentum exchange between the disk and the halo is mediated by the lower resonances, with the disk losing and the halo gaining the angular momentum. Overall, the resonances provide an independent test of the quality of the numerical scheme. When the N -body potential is too ‘grainy’, the particles cannot be locked by the resonances and so the latter efficiency in redistributing the angular momentum is sharply reduced.

2.1. Initial conditions

The main challenge in running evolutionary models of galactic disks embedded in triaxial halos is to form the initially stable halo configurations in the first place. A limited number of options known to us was not considered to be satisfactory, as they did not allow for a suf-

⁴ By ‘fast rotating bar’ we mean a bar which extends to about its corotation radius

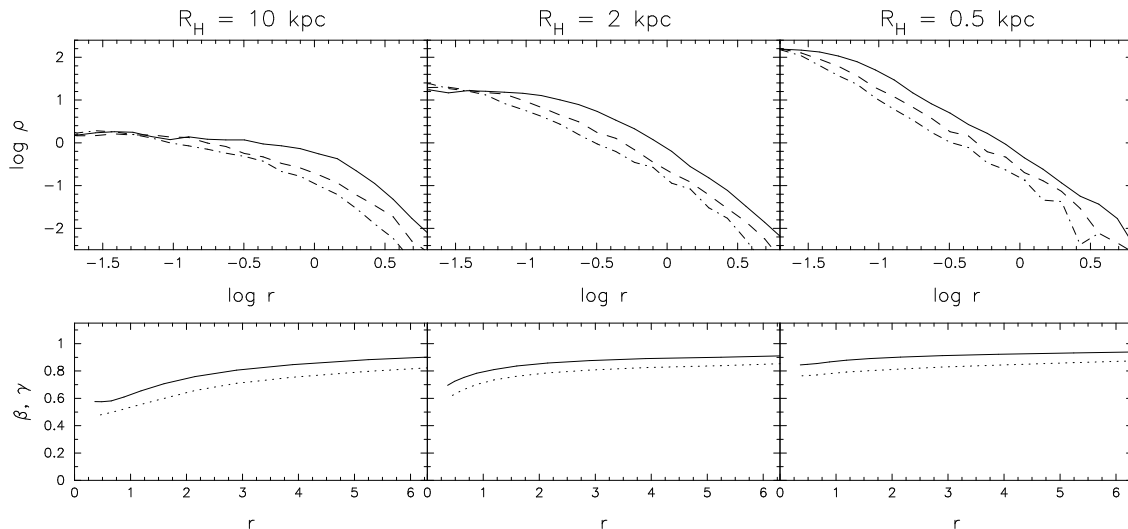


FIG. 1.— *Top panels:* Density distribution of the *live* triaxial halos along its principal axes (solid line: along a , dashed line: along b , dotted line: along c -axis) for models with a varying core size, R_H . *Bottom panels:* Potential axes ratios $\beta = b/a$ (solid line) and $\gamma = c/a$ (dotted line) for the same models.

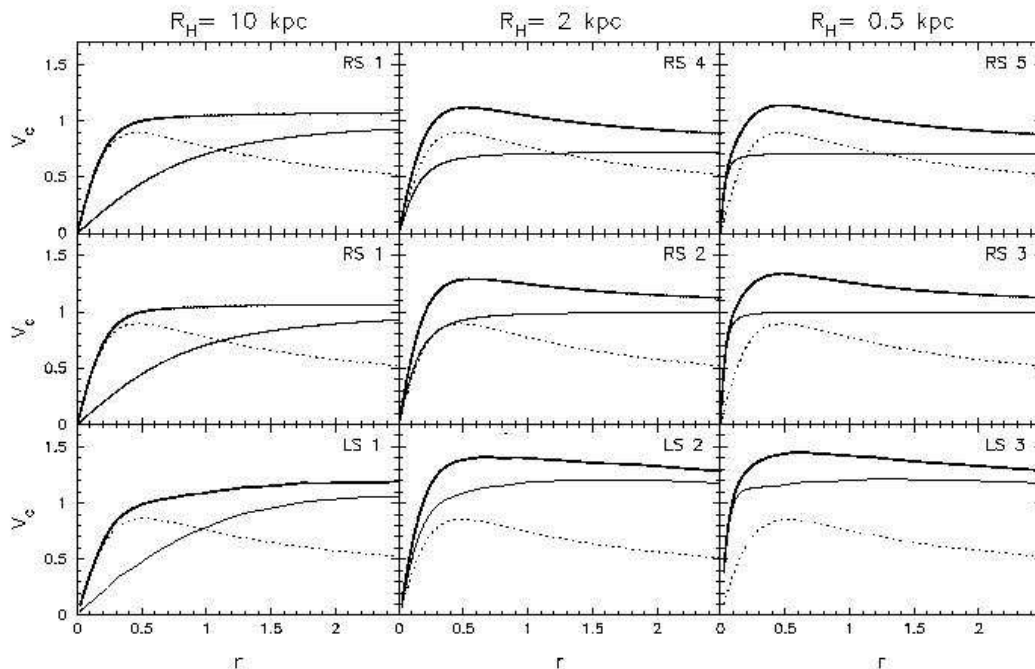


FIG. 2.— Initial rotation curves for (*upper panel:*) RS1, RS4 and RS5 models (rigid spherically-symmetric halos, constant M_D/M_H) within $r = 10$ kpc; (*middle panel:*) RS1 to RS3 models (rigid spherically-symmetric halos, constant V_H); and (*lower panel:*) LS1 to LS3 (live axisymmetric halos) with cores of 10, 2 and 0.5 kpc. Thin solid line shows halo contribution, dotted line — disk contribution, and thick solid line — the total. The units of length and velocity correspond to our model units.

ficient control of initial triaxiality and mass distribution in the halos. Instead we have designed the following procedure to obtain the required halo properties, which is described below.

First, we have used the known density-potential pairs of required symmetry to lay out particles up to some given radial cut-off radius. The velocity distribution function has been taken $\propto E^{-\alpha}$, where E is the energy and $\alpha = 2.5 - 3.5$, i.e., below the 3.5 value for the Plum-

mer sphere. Next, the halo has been evolved for about $50 \tau_{\text{dyn}}$ to allow for any residual relaxation to cease. This has resulted in a stable spherically-symmetric configuration. For the axisymmetric halos, a *frozen* stellar disk has been gradually introduced thereafter and the halo has been given time to relax again in this growing disk potential. The disk potential slightly changes the initial halo core size and therefore we apply an adiabatic cooling procedure to the halo particles within the core region,

TABLE 1
INITIAL MODEL PARAMETERS

Model	$R_{\text{H}} [kpc]$	V_{H}	β	γ	Notes
RS 1	10.0	1.0	1.0	1.0	Rigid spherically-symmetric halo
RS 2	2.0	1.0	1.0	1.0	Rigid spherically-symmetric halo
RS 3	0.5	1.0	1.0	1.0	Rigid spherically-symmetric halo
RS 4	2.0	0.721	1.0	1.0	Rigid spherically-symmetric halo
RS 5	0.5	0.708	1.0	1.0	Rigid spherically-symmetric halo
LS 1	10.1	1.13	1.0	0.99	Live axisymmetric halo
LS 2	1.8	1.18	1.0	0.98	Live axisymmetric halo
LS 3	0.3	1.20	1.0	0.98	Live axisymmetric halo
RT 1	10.0	1.0	0.9	0.9	Rigid triaxial halo
RT 2	2.0	1.0	0.9	0.9	Rigid triaxial halo
RT 3	0.5	1.0	0.9	0.9	Rigid triaxial halo
RT 4	2.0	0.719	0.9	0.9	Rigid triaxial halo
RT 5	0.5	0.708	0.9	0.9	Rigid triaxial halo
LT 1	10.5	1.14	0.79	0.72	Live triaxial halo
LT 2	2.4	1.19	0.84	0.77	Live triaxial halo
LT 3	0.5	1.19	0.88	0.79	Live triaxial halo
LT 3 HM	0.7	1.10	0.84	0.77	as LT 3, but with half-mass disk
LT 3 MT	0.5	0.4	0.9	0.8	as LT 3, but maintaining triaxiality

NOTE. — Columns: (1) model type (see text); (2) (fitted) halo core radius; (3) (fitted) constant in eq. 1; (4) (fitted) halo equatorial axial ratios; (5) (fitted) halo polar-to-longest axis ratios

by gradually reducing the velocities. Before introducing the disk for the triaxial cases, we have implemented a similar adiabatic ‘heating-cooling’ procedure to the halo particles to create a triaxial halo of required flatness and prolateness, by using ‘heating’ of the velocities along the x -axis and ‘cooling’ along both the y - and the z -axes, over some period of time, i.e. some $40 \tau_{\text{dyn}}$. The fractional energy heating/cooling per dynamical time is very small, $\sim 10^{-6}$ per machine timestep (corresponding to about 10^{-5} per dynamical time), so the system is never taken out of a dynamical equilibrium. The disk potential partially dilutes the halo triaxiality and therefore we apply a second heating-cooling procedure after the disk has been introduced in the models. This finally results in both the required $\beta = b/a$ and $\gamma = c/a$ distributions and core sizes in the halo potential (Fig. 1). Note that in the models with smaller cores it is more difficult to impose (and maintain) the triaxiality at all radii.

For a direct comparison with ES02 in this work, we aimed to closely reproduce their initial conditions. A 3-D mass distribution (live or analytical) which pairs with the nonrotating logarithmic potential, Φ_{H} , (e.g., Binney & Tremaine 1987) was used for the halo,

$$\Phi_{\text{H}} = \frac{1}{2} V_{\text{H}}^2 \log (R_{\text{H}}^2 + x^2 + \beta^{-2} y^2 + \gamma^{-2} z^2) , \quad (1)$$

where V_{H} is the asymptotic (in the limit $R \gg R_{\text{H}}$ and $\beta, \gamma \rightarrow 1$) circular velocity, R_{H} is the halo core radius and $\beta (= b/a)$, $\gamma (= c/a) < 1$ are the azimuthal and polar potential axis ratios. Note that the corresponding mass distribution is diverging for this potential. We, therefore, applied a truncation radius for models with live halos, i.e. 50 and 100 kpc for the axisymmetric and triaxial halos, respectively. Although the potential of these models is going to change, both as a result of the disk addition and, in the case of live halo response, to the disk evolution, we find it nevertheless beneficial to compare the evolving potential to the fitted logarithmic one. For spherical (axisymmetric) models $\beta = \gamma = 1.0$,

while for triaxial models $\beta = 0.9$ and $\gamma = 0.8$, approximately for live models, after the halo has relaxed in the disk potential.

We have used two sets of initial halo models. In the *first set*, $1 \rightarrow 4 \rightarrow 5$ (see Table 1) — for rigid halos only — we adjust V_{H} requiring 1 : 1 ratio of halo-to-disk mass within $r = 1$. This means that on the scale of $r \sim 1$ models with different core size have the same mass concentration. On smaller scales of course the more cuspy models will be always more centrally concentrated, which can affect the properties of developing stellar bars.

In the *second set*, $1 \rightarrow 2 \rightarrow 3$, for which we run both rigid and live models, we retain the value of V_{H} , obtained for an axisymmetric halo with a core radius of $R_{\text{H}} = 1$. For further halo configurations, the total halo mass within its truncation radius $r = 100$ kpc, is 10.0 in our units. Thus, when moving from a large flat core to cuspy models, we move from a maximal disk model to a halo-dominated one.

Similarly, as in ES02, the stellar disk has been set up following the potential in the form of (Miyamoto & Nagai 1975),

$$\Phi_{\text{D}} = - \frac{G M_{\text{D}}}{\sqrt{x^2 + y^2 + \left(A_{\text{D}} + \sqrt{B_{\text{D}}^2 + z^2} \right)^2}} , \quad (2)$$

which describes a disk-bulge system, with the parameters $A_{\text{D}} = 0.284$ and $B_{\text{D}} = 0.05$, determining the scalelength and height, respectively. The disk mass is 0.5 within $r = 1$ and about 0.6 within the disk cut-off radius, i.e. $r = 2.5$. The initial Toomre’s Q parameter is taken 1.2 and constant with radius. The disk rotational velocities in triaxial halos have been set using our standard procedure but ignoring the mild triaxialities in the total potential. The initial models are summarized in Table 1 and the initial rotation curves are shown in Fig. 2.

3. RESULTS

We now present the bar evolution and its interaction with the outer disk and halo for the numerical models listed in Table 1. We start with disks in rigid axisymmetric⁵ halos and compare them with those in rigid triaxial halos, assuming constant disk-to-halo mass ratios within 10 kpc, and varying the flat core sizes from large 10 kpc to cuspy ones. We then continue with live axisymmetric and triaxial halos.

3.1. Comparing Bars in Rigid Axisymmetric and Triaxial Halos with Constant Disk-to-Halo Mass Ratios

3.1.1. Rigid axisymmetric halos

Only circumstantial evidence exists comparing the bar formation and evolution in analytical (i.e., rigid) and live halos, even in the case of an axial symmetry (e.g., Christodoulou, Shlosman & Tohline 1995 and refs. therein), with the exception of Athanassoula (2002). It is known that rigid halos are less hospitable to bar growth. All equal, bar instability in this case requires larger disk-to-halo mass ratio than in the live halo systems. This behavior of stellar disks embedded in non-responsive halo potentials can be readily understood in terms of absence of (resonance) halo orbits capable of absorbing the disk angular momentum. As expected, it is accompanied by a nearly constant bar pattern speed, as the angular momentum loss from the bar is minimized to the outer disk only.

Fig. 3 exhibits some properties of stellar bars in such rigid axisymmetric (RS) halos — with a large flat-core $R_H = 10.0$ kpc (model RS 1), a smaller core $R_H = 2.0$ kpc (model RS 4) and a cuspy (model RS 5; $R_H = 0.5$ kpc) density profile (see Table 1). The (normalized) amplitude of the $m=2$ mode, A_2 (Fig. 3, top panels) provides only a partial description of the bar evolution. Because it is an integrated quantity over some specific radius and because the bar sizes will differ from model to model, it does not allow for a direct comparison between bars in different models. One can encounter a small size but strong bar whose amplitude will be diluted (say) by a large averaging region. To resolve this dilemma, we use both the bar amplitude, measured within a thin cylinder of radius of 5 kpc, and the bar length and its maximum ellipticity, $\epsilon = 1 - b/a$ (obtained from the isodensity fits, in the plane (Fig. 3, middle panels), to characterize its strength. Both approaches can be tested observationally.

We note that a reliable determination of a N -body bar size from isophote fitting has its pitfalls (see Martinez-Valpuesta & Shlosman 2004). Before the vertical buckling, the bars have a flat distribution of ellipticity with radius, while at later times the ellipticity has a clear maximum. We find empirically that a good approximation to the bar size would be the radius where the bar ellipticity drops by 0.1. This is verified using nonlinear orbit analysis, finding the x -extent of the largest stable x_1 orbit in the bar (Martinez-Valpuesta, Shlosman & Heller 2006). On the other hand, the ellipticity of the surrounding disk shows a gradual decline with radius, even in mildly triaxial halos used in this work. This different behavior of

ellipticity in numerical bars and disks allows us to safely separate them.

The rigid axisymmetric halo models RS 1, 4 and 5 have been arranged along the same sequence of decreasing core size as in Fig. 2. These models have the same disk-to-halo mass ratio within the central 10 kpc, but correspond to increased central concentration in the halo.

All three models develop a strong bar in the process of a ‘normal’ bar instability (Fig. 3). The bar amplitudes, A_2 , show a strong peak after the initial bar growth, at $\tau \sim 30 - 50$, and a subsequent decline, partly associated with a transient $m = 3$ mode A_3 . The latter appears to be a purely numerical artifact resulting from mixing of analytical (halo) and live (disk) potentials. The more centrally-concentrated models suppress the (planar!) $m=3$ mode more efficiently. The sudden weakening and shortening of the bars has been related to the onset of chaos in strong bars (Martinez-Valpuesta & Shlosman 2004), which can be the case in these models as well. Asymptotically, the more cuspy models show marginally stronger bars. While the RS4 bar exhibits a slight secular growth in A_2 , the RS 5 bar shows a secular decline at the same time, again probably related to stronger chaos excited in cuspy models.

The asymptotic bar size, $\sim 6 - 7$ kpc, is largest in RS 1 — the large halo core model, and about $3 - 4$ kpc in RS5. The *maximal* bar size (at $\tau \sim 30 - 50$) also clearly correlates with the halo core size, R_H . This trend is much more pronounced in models which have increasing central mass concentration (see section 3.2.1 and Fig. 5). The bar ellipticity, ϵ , closely follows the size evolution of the bars in all models. The bar pattern speed, Ω_p , shows some initial decline with time, more substantial in cuspy models, but then levels off — as expected, because of lack of angular momentum absorbing material in axisymmetric and to a certain degree also in mildly triaxial halos. The outer disk quickly saturates for this redistribution of angular momentum. As expected, more cuspy models have progressively faster Ω_p .

We find that the bars in rigid halos are not subject to the buckling instability (e.g., Pfenniger & Friedli 1991), apparently because of difficulty to develop vertical asymmetric modes, $m = 1$. But vertical $m = 3$ and 5 show up progressively more in RS 4 and RS 5, at the level of $\sim 8\%$. The vertical resonant heating in the bar (e.g., Friedli & Pfenniger 1990) is not obviously observed, possibly due to the rigid potential of the halo, and especially due to the absence of a discreteness noise in the analytical potential.

The effect of the bar on the disk is to shorten the original radial scalelength in the inner (bar region) disk and in the outer disk. In this sense, the combination of initial conditions and disk evolution maintain a double-exponential disk, r_D , characterized by the inner and outer radial scalelengths. The inner disk (the bar region) in RS 1 develops $r_D \sim 2.2$ kpc, when measured along the bar major axis. This value is progressively smaller for more cuspy models, e.g., ~ 1.6 kpc in RS 5. In the outer disk, r_D decreases from its initial value 5.7 kpc to about 5 kpc with time and remains constant when disk/bar reaches quasistationary stage after $\tau \sim 80$ (in RS 1). The Toomre’s Q increases overall from 1.2 to 2.1, measured at two radial initial scalelengths after the bar weakening in RS1 and more so in RS 4 and RS 5.

⁵ We are interested only in this property of spherical halos and refer to them as axisymmetric

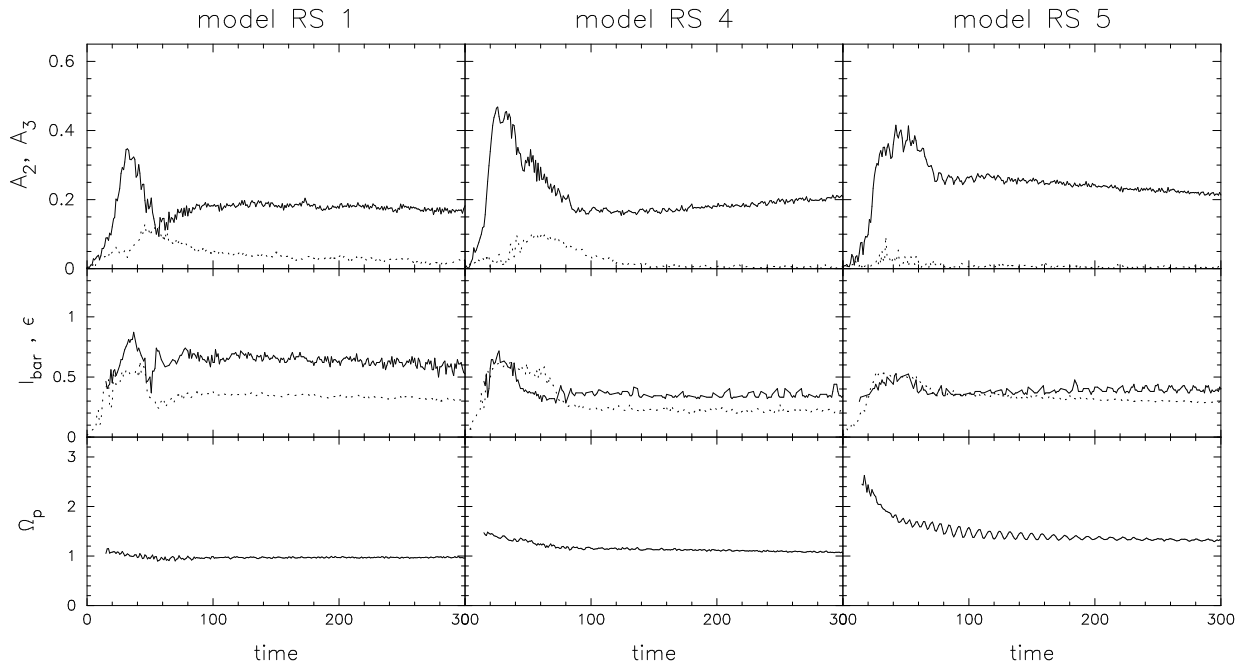


FIG. 3.— Bar strength (top panels; $m = 2$ amplitude A_2 : solid line, $m = 3$ amplitude A_3 : dotted line), bar length and (max.) ellipticity (middle panels; solid and dotted line, respectively) and pattern speed Ω_p (bottom panels) as a function of time for models RS 1, 4 and 5 (from left to right) with rigid axisymmetric halos.

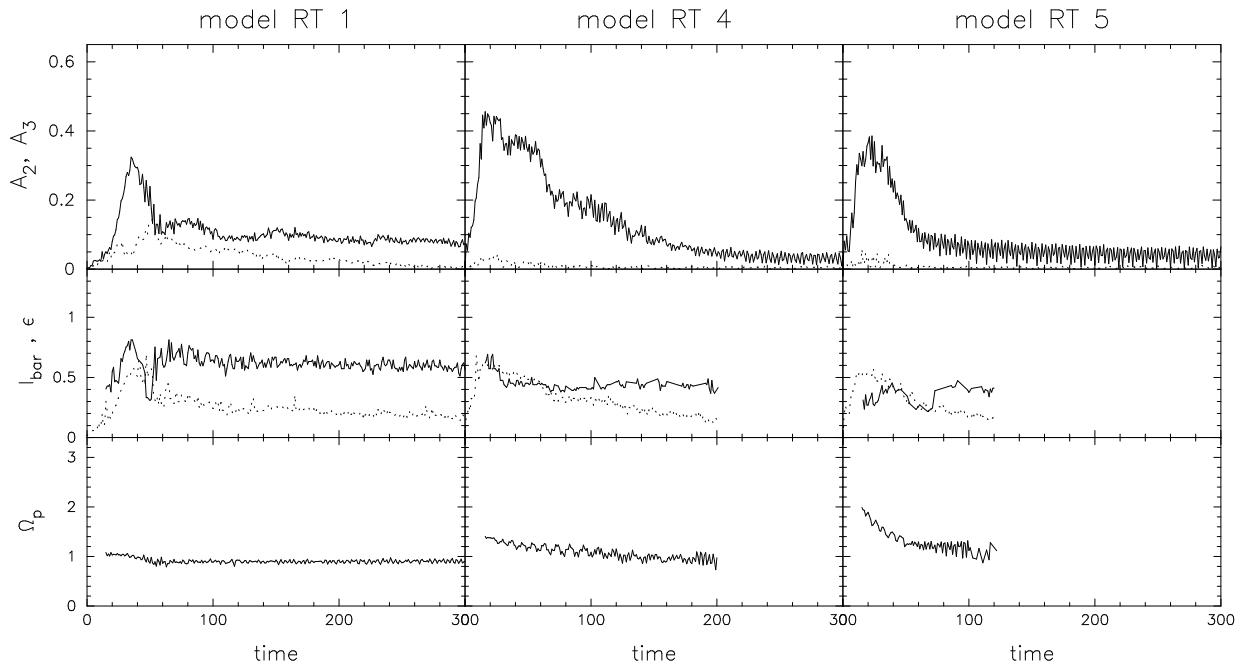


FIG. 4.— Same as Fig. 3, but for models with rigid triaxial halos, i.e. RT 1, 4 and 5 – constant mass ratio within 10 kpc.

The vertical disk scaleheight, z_D , shows progressively less change with increased cuspsiness. While it increases from 0.5 kpc to ~ 0.7 kpc in RS 1, as a result of disk heating, towards the end of the simulations, it increases only 0.6 kpc in RS 4 and stays unchanged in RS 5.

3.1.2. Rigid triaxial halos

In this section we describe the evolution of the models with rigid triaxial halos and a constant M_D/M_H within 10 kpc (Table 1), i.e. models RT 1, RT 4 and RT 5. Some of the bar properties in these models are shown in Fig. 4. The angular momentum redistribution is discussed in section 4.

The bar initial growth and size, its maximal strength (i.e., of A_2), and even its peak ellipticity in rigid triax-

ial halos are remarkably similar to those in axisymmetric ones. The only difference is that the growth rate is faster and so the peak strength is achieved earlier. The subsequent evolution, however, is very different — the bar dissolves over the characteristic time of $\sim 30 - 100$, depending on the model, leaving only a weak oval distortion behind (Fig. 4). The general trend of bar evolution in this sequence of models clearly links the halo cuspieness to the dissolution process, which is amplified by the halo triaxiality — a trend predicted by ES02 based on the orbital stability analysis and the development of connected chaotic domains in these models

The bar size plot (mid panels), which indicates a bar of 6 kpc in RT 1 at later times, is misleading here and seems to represent only the disk response to the triaxial potential and the ellipticity is that of the disk. As long as the bars exist in these models, their pattern speeds mirror those in axisymmetric halos of the same mass concentration.

Despite the destruction of bars in RT 1 to RT 5 models, the disk tends to acquire a double-valued radial exponential scalelength: the inner one of about 2 kpc and the outer one of $\sim 5-6$ kpc. The Toomre’s Q and the vertical scaleheight behave as in the axisymmetric sequence.

3.2. Comparing Bars in Rigid and Live Axisymmetric Halos with Decreasing Disk-to-Halo Mass Ratios

3.2.1. Rigid axisymmetric halos

To provide a more direct comparison to the results of ES02, we present in this section a set of simulations in which we closely follow their model parameters. The basic difference with the previous set of models is that halo mass within the central 10 kpc is increased for progressively smaller cores (Table 1). Thus, when moving from flat core to cuspy models, we move from a maximal disk model (RS 1) to a halo-dominated one (RS 3) as evident from Fig. 2. Fig. 5 shows the evolution of stellar bars in such rigid axisymmetric halos. This corresponds to the increased central concentration, in excess of that shown by RS 1→RS 4→RS 5 sequence.

Fig. 5 exhibits the disk evolution inside such halos. The strong bar only develops in the model RS1. The RS2 suppresses the bar growth for the first $\tau \sim 60$, developing a short, $\sim 2-3$ kpc bar. Thereafter, A_2 drops and the bar further weakens to a rather oval distortion which persists over the period of simulations. The RS3 suppresses the bar growth rate even stronger, and A_2 shows a steady secular growth not leveling off even after $\tau \sim 300$, while A_3 is completely suppressed in a more cuspy models.

Q increases to ~ 2 while the vertical scalelength shows no change whatsoever. The bar pattern speed correlates with the halo’s mass concentration, i.e. increasing with smaller core sizes. Pattern speed in RS 3 is linearly decreasing with time reflecting the secular increase in A_2 .

To summarize the sequence of rigid axisymmetric halos RS 1→RS 3: the stellar bar is basically suppressed in more cuspy models in accordance with ES02 analysis.

3.2.2. Live axisymmetric halos

Models LS1 to LS3 present the case of live axisymmetric and increasingly cuspy halos. After introducing the disk and letting the halo to relax, we have fitted the halo density profile at the end of this relaxation process

using the parameters of logarithmic potential, V_H , R_H , β and γ (see Table 1). The new density profiles for the halo can be fit reasonably well and show slight increase in V_H and unchanged β . Owing to the flattened disk potential γ slightly decreases. For model LS 1, the core radius remained at ~ 10 kpc, for model LS 2 it decreased to ~ 1.8 kpc, and for model LS 3 — to some 0.3 kpc. The main difference between these models and the previously discussed ones with rigid halos, however, is an active redistribution of angular momentum between the bar forming region in the disk and the live halo (see section 4). For all live axisymmetric halos during disk evolution the halo density profile is stable (e.g., as shown for LS3 in Fig. 7).

The sequence LS 1→LS 3 has produced the strongest bars among all of our models (Fig. 6). The amplitude A_2 has also shown a pattern of behavior: (1) the bar growth is fastest in LS 1 (disk dominated) and slowest in LS 3 (halo dominated); (2) the maximal bar strength is increasing along the sequence; (3) all bars exhibit vertical buckling, (4) A_2 decays most strongly in LS1 after the buckling, and least in LS 3; and finally (5) the post-buckling bar in LS 1 continuous its secular growth, which quickly saturates in LS2 and starts to decay in LS3. Hence LS 1 (and to a lesser degree LS 2) shows most resemblance to the secular evolution of a stellar bar in Martinez-Valpuesta, Shlosman & Heller (2006) where the bar weakens dramatically during its buckling and increases its strength thereafter.

For model LS 1, the bar size decreases from roughly 10 kpc just before the buckling, to ~ 7 kpc at $\tau \sim 60$ and then increases again to about 9 kpc after the buckling. For model LS 3, it grows from 5 kpc to 8 kpc. This means that during the initial growth, up to the time of the buckling, the bar is confined to the regular region delineated in ES02.

The bar sizes show clear correlation with the halo core size, R_H , as in the rigid sequence RS1 → RS5 described in section 3.1. One can clearly observe here the ‘delay’ in the bar growth in halo-dominated models. The bar ellipticity shows a visible decay after the buckling in LS1 and stabilizes afterwards, while in LS 2 and LS 3 ϵ does not decay.

As expected, the bars slow down substantially over the simulation time and the initial slowdown is well correlated with R_H (Fig. 6, bottom panels). This angular momentum transfer from the disk is deposited mostly in the internal circulation in the halo as its figure does not acquire rotation (section 4).

We have mentioned above that all LS models show buckling which is less pronounced for halo-dominated models. This can be noted from the amplitudes of the vertical modes — LS 1 shows clear increase of $m=1$, and LS 2 and 3 only in $m=3$ and 5.

The disk evolution in LS models again leads to a double-exponential scalelength: the inner bar-dominated part has r_D which slightly decreases from LS1 to LS3, from ~ 2 kpc to ~ 1.6 kpc, while the outer disk scalelength actually increases along the sequence, from about 5 kpc to just below 6 kpc.

The disk scaleheight in LS1 shows an abrupt increase at $\tau \sim 50$ from its initial value 0.5 to about 0.9 kpc within few dynamical times, during the vertical buckling of the bar. This effect is clearly related to the formation of a

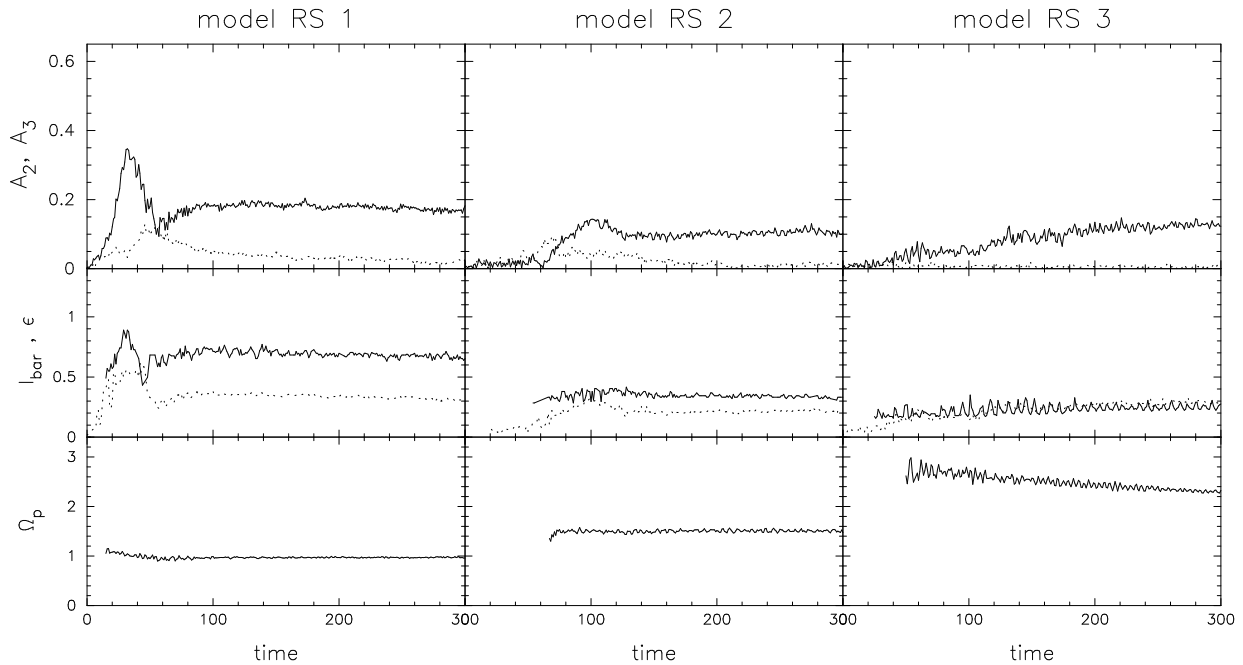


FIG. 5.— Same as Fig. 3, but for models with rigid axisymmetric halos, i.e. RS 1, 2 and 3 – from disk to halo dominated.

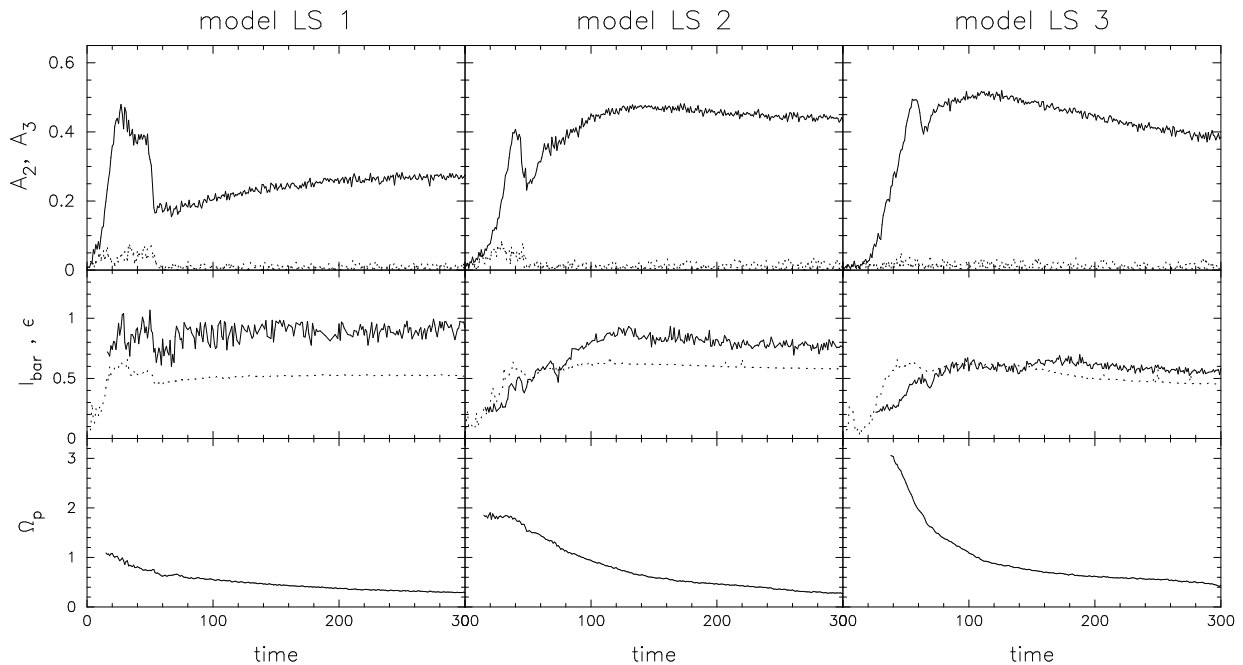


FIG. 6.— Same as Fig.3, but for models LS 1–3 with live axisymmetric halos.

pseudo-bulge, i.e., bulge of a boxy/peanut shape. LS 2 experiences a milder increase in z_D to ~ 0.65 kpc and in LS 3 it remains largely unchanged.

All LS models show the formation of pseudo-bulges associated with the vertical buckling of the bars. However the shapes of these bulges differ and this difference persists for the time of the simulations. While in model LS 1 and LS 2 the isodensity contours show a more boxy shape, the cuspy model, LS 3 develops a peanut-shaped

bulge (see also Athanassoula & Misiriotis 2002).

3.3. Comparing Bars in Rigid and Live Triaxial Halos

3.3.1. Rigid triaxial halos

The RT 1→RT 3 sequence describes the disk evolution within rigid triaxial halos with decreasing core size, closely following the initial conditions in ES02 (Fig. 8). The only difference between the previously discussed RT1→RT5 sequence and RT 1–3 is that the latter one

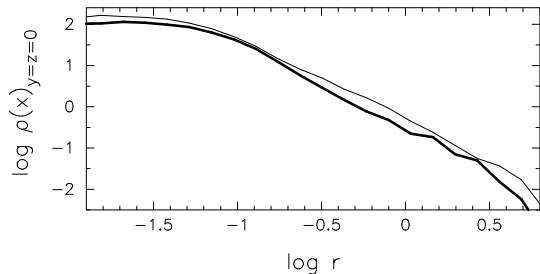


FIG. 7.— Density profile along the halo main (longest) axis for time $t = 0$ (thin line) and $t = 300$ (thick line) for model LS3 ($r_H = 0.05$).

is progressively halo-dominated. This difference is responsible for the damping of bar instability in a disk embedded in RT2 and RT3 halos. Even RT1 shows a substantial decay of the initially strong bar to a largely an oval distortion, unlike the bar in RS1 model. Hence, asymptotically RT2 and RT3 behave as RT4 and RT5. However, early in the disk evolution, the former models show strong bars (see section 3.2.1).

The size and ellipticity of the central (bar) oval distortion in RT1 to RT3 correlate well with R_H . In RT1, the maximal bar length is ~ 9 kpc at $\tau \sim 35$ and after $\tau \sim 50 - 60$, the bar deteriorates into a rather triaxial (in the equatorial plane) configuration within the central $r \sim 4 - 5$ kpc. Note the A_2 amplitude becomes finite already in the first moments into the simulation because of the disk response to the halo triaxiality.

The first few disk rotations, especially in RT2 and RT3, show a grand design spiral structure in the outer disk which remains tightly bound and quickly decays. Even more than in RS3, the disk stays largely axisymmetric within the central few kpc after $\tau \sim 30$. Its surface density profile shows (almost) no evolution. The outer disk radial scalelength decreases to about 4.5–5 kpc, while the disk scaleheight stays unchanged.

3.3.2. Live triaxial halos

As in the case of the live axisymmetric halos, the triaxial halos are modified by the introduction of the frozen disk potential. At the moment of disk ‘release,’ the halo core size in model LT1 has slightly increased to $R_H \sim 10.5$ kpc, in LT2 it has increased to ~ 2.4 kpc, and in LT3 stayed at 0.5 kpc (see Table 1). We found it increasingly difficult to maintain the (inner) halo triaxiality in cuspy models after introduction of a frozen disk. This has affected the LT3 model which possesses a more structurally unstable halo.

The evolution of A_2 amplitude in the LT1→LT3 sequence is remarkably different from that in the rigid sequence RT1 to RT3. The initial disk response to the halo potential has induced strong bars in all these models. The fate of the bar, however, differs depending on the model. The bars decay nearly linearly in LT1 and LT2 on a timescale of $\tau \sim 100$, and enter a steady state in LT3. Overall, the LT3 model behaves differently and its evolution resembles more the LS3 model, although the bar is not so strong. The buckling is clearly visible in all LT models. However, the resulting boxy shapes of bulges are quickly erased in LT1 and LT2, while peanut shape

bulge in LT3 persists till the end of the simulation. The planar A_3 amplitude is negligible in all live halo models.

The radial density profile in the triaxial halo is stable during live disk evolution in all these models, even for the cuspy LT3. However the halo triaxiality T is reduced sharply in LT3, due to decrease in ϵ_H . After $\tau \sim 70$, it has largely lost its prolateness, $\beta \sim 1$ (Fig. 10). This halo axisymmetrization is only partially a result of initial conditions — LT3 has had somewhat larger β at $\tau = 0$, as noted above. Rather, as we discuss in section 5, the halo is much more structurally unstable in cuspy models. In order to test this latter assumption, we have re-run the LT2 model with a *frozen* disk. Fig. 11 shows the resulting evolution of potential axial ratios for the halo. Both halo flatness, f , and its prolateness, ϵ_H , show no evolution over 300 dynamical times, ~ 14 Gyrs. This confirms that it is the developing bar perturbation which decreases the halo prolateness without much effect on its flatness.

The bar size and ellipticity LT1 and LT2 (Fig. 9) represent a combined disk and bar evolution. The outer disk develops elaborate system of long-lived spiral arms, much more pronounced than in live axisymmetric models. Because of the difficulty to disentangle between the bar, spiral arms and the oval disk, the estimated bar size in Fig. 9 is erroneous. The inner disk radial scalelength shows a general decrease to about 1.7 kpc in LT1 and to ~ 1.8 kpc in LT2 and LT3. The outer disk has r_D approaching ~ 4.8 kpc in LT1 and about 5–5.5 kpc in LT2 and LT3. The inner disk scaleheight increases abruptly to ~ 0.9 kpc after $\tau \sim 35$ in LT1 and to ~ 0.8 kpc in LT2 and ~ 0.75 kpc LT3 models.

The live triaxial models are especially efficient in triggering the spiral structure in the barred disk. The arms penetrate deeper towards the center in LT2 model with smaller core radius. The strength of the spirals depends on the position angle of the bar with respect to the longest halo axis — when the bar is normal to this axis, the spirals are prominent. This type of spiral regeneration happens as long as the bar exists.

3.3.3. Models with continuous support for halo triaxiality

Models LT1 to LT3 show that the disk (and bar) response to a live triaxial (halo) potential can act as to decrease its prolateness, e.g., equatorial ellipticity. This effect is most pronounced in model LT3, where it has been difficult to induce the halo’s triaxiality, especially in its central region. Compared to the models with larger cores, the disk in LT3 evolves more similarly to that in axisymmetric halos. Because of the strong feedback of stellar bars onto the halo triaxiality, we have run a model for LT3 with a continuous support for triaxiality — the LT3MT model. The simple justification for this is that mergers will induce triaxiality in the extended DM halos in the first place. We, therefore, mimic this process by maintaining or continuously regenerating a mild halo triaxiality, and at the same time allowing the live halo to interact with the live disk.

Fig. 12 (right) exhibits such an evolution of LT3MT and provides A_2 from LT3 for a comparison. The adiabatic heating/cooling procedure was gradually turned on and has its full strength from $\tau = 70$ to 225, when it is gradually turned off. Initially, the LT3MT evolved

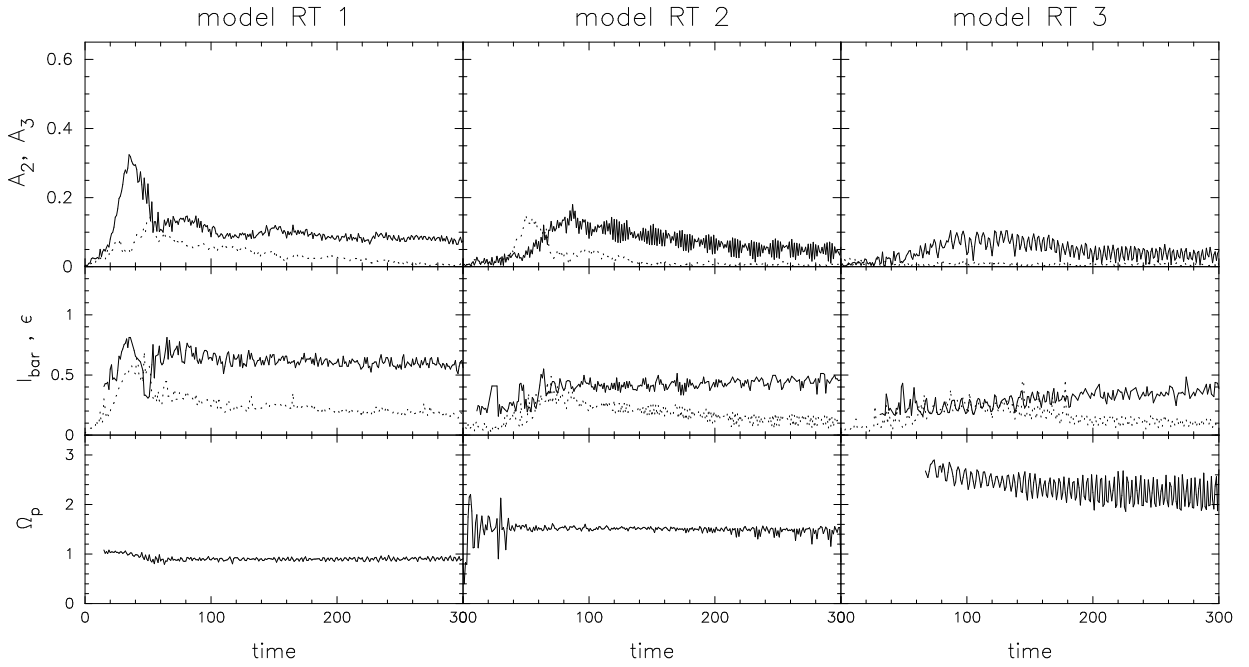


FIG. 8.— Same as Fig. 3, but for models with rigid triaxial halos.

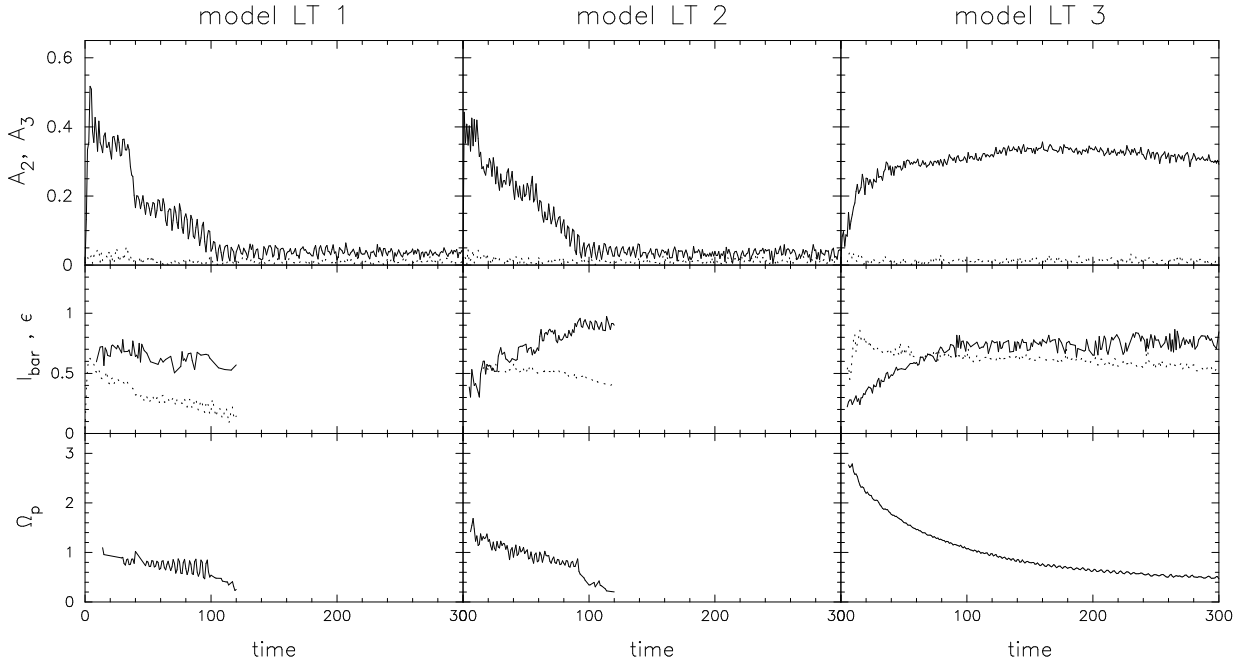


FIG. 9.— Same as Fig. 3, but for models with live triaxial halos.

identically to LT3. Because the halo triaxiality has been maintained at the steady level (Table 1), it has a profound effect on the disk. The bar completely dissolves and starts to grow afterwards when the triaxiality is gradually washed out.

3.3.4. Light disks in triaxial halos

The interaction between the halo and the evolving disk tends to gradually wash out the initial triaxiality in the

halo. The efficiency of this process depends on the disk-to-halo mass ratio. The bar is then able to grow within the region in which the halo becomes more axisymmetric. To show explicitly the dependency of halo and disk evolution on their (inner) mass ratios, we have run live triaxial models with lower disk-to-halo mass ratio within central 10 kpc for the cuspy LT3 model. Here we show only LT3HM — the model with a half disk mass. The bar instability in this model is substantially suppressed

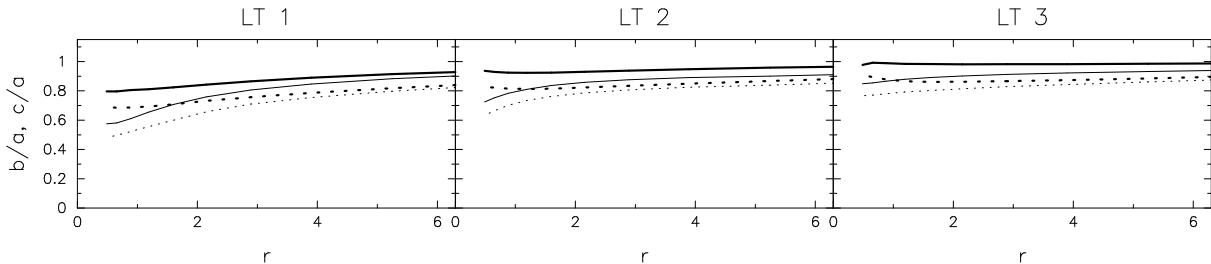


FIG. 10.— Halo (isopotential) axes ratios β (full lines) and γ (dotted lines) as a function of radius for models with live triaxial halos. Thin and thick lines indicate the profiles at the beginning and the end ($t=300$) of the runs, respectively.

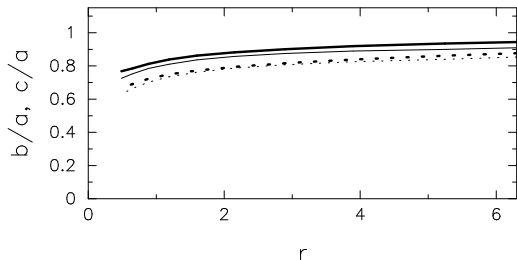


FIG. 11.— Testing the halo evolution in the LT2 model: re-run of the model with a *frozen* instead of the live disk, for comparison. Axes-ratio β (full line) and γ (dotted line). The thin and thick lines represent the times $t=0$ and $t=300$, respectively. The absence of evolution in β and γ in this case confirms that the evolution observed in Fig. 10 results from interaction between the disk and the halo.

compared to LT 3 model. LT 3HM develops a weak oval distortion in the center (Fig. 12, left) whose shape depends strongly on its orientation with respect to the halo major axis — its ellipticity is smaller when it is normal to the halo, and larger, when it is parallel. Otherwise, the disk is stable and no bar instability develops.

4. DISK-HALO ANGULAR MOMENTUM EXCHANGE

The general direction of the angular momentum flow in all models is expected to be from the inner bar-forming disk towards the outer disk and the halo. This reflects behavior of all models that break their axial symmetry for whatever reason, that of initial conditions (triaxial halos) or as a result of a spontaneous bar instability. However, when this redistribution is mediated by the bar, there is also an additional flow from the inner disk (inside the bar corotation) to the outer disk.

In the models with rigid axisymmetric halos the exchange of angular momentum is limited to that between the inner and outer disks, across the corotation and mediated by the bar. Models RS 1 and RS 5 (Fig. 13) show that the total loss of the angular momentum from the disk is $\Delta L_z = 0$ and that the outer disk gains the angular momentum from inner part. This gain is larger for RS 5 as it develops stronger bar. Rigid triaxial models drain some of the angular momentum from the disk (e.g., RT 5 in Fig. 13) but this does not dominate the L -exchange because of the mild triaxiality here.

Fig. 14 shows the effect of introduction of a live halo, axisymmetric and triaxial. The total loss of the L by the disk has been dramatically amplified compared to the rigid triaxial halos. The outer disk still gains the

same amount but most of L goes to the halo. The strong and long-lived bar developing in the LS1 model is instrumental in this transfer. The main difference with the LT1 model is that the disk immediately acquires a strongly oval shape which is gradually lost and so overall the transfer amount of angular momentum is less than in LS1. However, during the first 20–30 dynamical times, the L -transfer is stronger in LT 1. Subsequently, the bar which has developed in LT 1 dissolves, which levels off the rate of angular momentum transfer.

Furthermore, in order to test the effect of the resonance coupling between the disk/bar and the halo, we have performed the spectral analysis of the orbital motion (Binney & Spergel 1982) in conjunction with our nonlinear orbital finder algorithm (Heller & Shlosman 1996). We find that a fraction of disk particles in live axisymmetric halos is locked by the lower resonances, especially by the inner Lindblad resonance (ILR). A fraction of the halo particles is locked by the corotation resonance — hence ILR-CR resonance coupling. Following Athanassoula (2002), we have frozen the model potentials at times $\tau = 100$ and 150, and compared the angular momentum of individual particles at these times. Most of the angular momentum flow between the disk and the halo was mediated by this ILR-CR coupling. Particles trapped at $\tau = 100$ largely remained trapped at 150. This result shows that the adverse effect of the grainy N -body potential on the evolution in our models is limited, and the latter is driven by a chaotic dynamics instead.

5. DISCUSSION AND CONCLUSIONS

We have analyzed the formation and evolution of stellar bars in galactic disks embedded in rigid (i.e., analytical) and live axisymmetric and mildly-triaxial DM halos of a varying cuspidity. The nearly axisymmetric potential employed in our simulations allows us to focus on the development of bar instability *per se* and does not violate the overall dynamics and survival of the disks. Using tailored numerical simulations we aimed at testing and extending the predictions of El-Zant & Shlosman (2002, ES02) which employed the method of Liapunov exponents to address the fate of bars in analytical triaxial halos. Our simulations of live halos, unlike ES02, include the feedback between the disk, bar, and halo. We fully support the main conclusions of ES02 and provide some additional insight into the bar and disk evolution.

We start with summarizing our results and follow up with discussion — *first* based on the bar strength. In all cases we can separate the initial bar growth to its

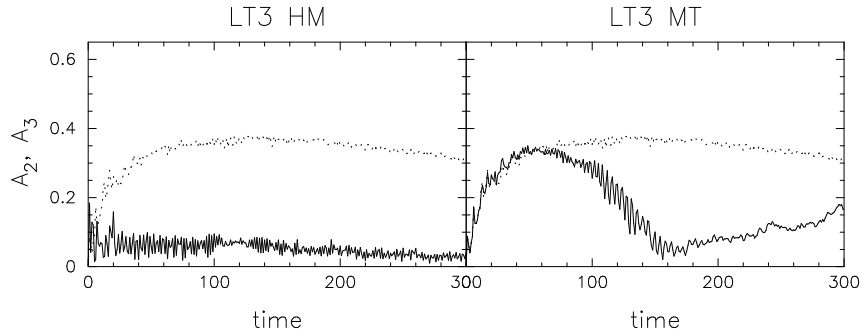


FIG. 12.— The bar amplitude A_2 for models LT 3 HM (0.5 kpc core) with a half mass disk (left panel) and LT 3 MT continuous support of triaxiality (right panel). The dotted line shows A_2 of LT 3 for comparison.

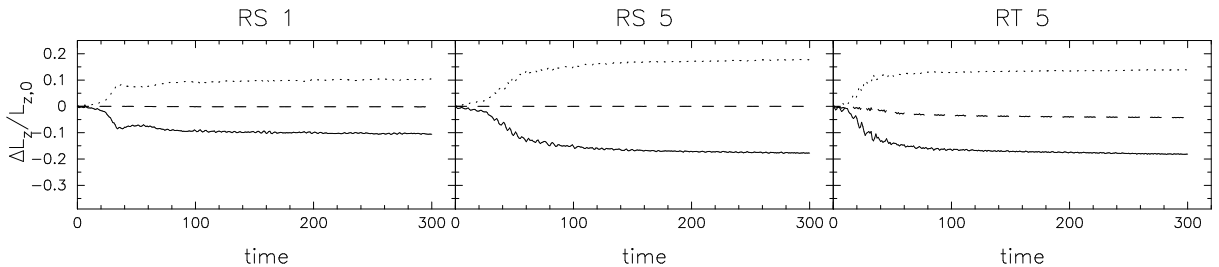


FIG. 13.— Models RS 1, RS 5 and RT 5 showing the angular momentum exchange in the live disk along the sequence with increasing cuspsiness and with a rigid axisymmetric (RS 1, RS 5) and triaxial (RT 5) halos. The change in the angular momentum in the disk, ΔL_z , is normalized by the total angular momentum in the disk, $L_{z,0}$, at $\tau = 0$ when it is released. The solid line represents integrated $\Delta L_z/L_{z,0}$ in the disk between $r = 0 - 10$ kpc, the dotted line — for $r > 10$ kpc and the dashed line — the change in the total angular momentum in the disk, which is absorbed by the halo.

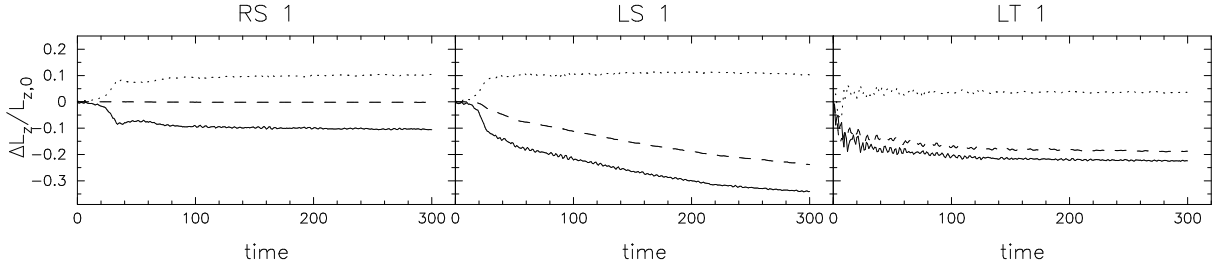


FIG. 14.— Models RS 1, LS 1 and LT 1 showing the angular momentum exchange in a rigid vs live axisymmetric vs live triaxial halos. As in Fig. 13.

full strength, over $\tau \sim 30 - 50 \sim 1.5 - 2$ Gyr, from the subsequent bar evolution, dynamical or secular, over the Hubble time. The first stage is very similar between all *rigid* axisymmetric and triaxial halo models. We find, that while some of the rigid halos suppress the bar formation, depending on the disk-to-halo mass ratio D/H within the disk radius, all live halos develop impressive bars with ellipticities in the range of $\sim 0.4 - 0.7$, depending on their evolutionary stage. In axisymmetric live cases (only!) these bars appear stronger for smaller D/H , in line with Athanassoula & Misiriotis (2002). In live halos, the bars develop faster in triaxial compared to axisymmetric halos. (This statement is marginally true also for rigid halos.)

All bars weaken at the end of the first stage. This process is accompanied by bar's vertical buckling in the live halos and formation of exponential (pseudo-) bulges of a peanut or boxy shape. No buckling is observed in

rigid halos.

The subsequent evolution of the bar differs substantially between axisymmetric and triaxial halos. In the former case, the bars appear dynamically stable and show a limited secular evolution by a factor of $\lesssim 2$ in strength, in growth or decay after the initial vertical buckling. This result is in agreement with Athanassoula (2002). In the latter case, the bars dissolve almost completely on a timescale of $\tau \sim 30 - 100 \sim 1.5 - 5$ Gyr, sometimes leaving behind a weak oval distortion in the central regions. This is true for all models with the exception of LT 3 — a live cuspy triaxial halo, where the triaxiality (i.e. prolateness) is erased early due to the feedback from the bar and its ensuing evolution closely resembles that of the axisymmetric halos.

To verify that the bar endurance is related to the erasure of the halo prolateness, we have run a test model where (live) halo triaxiality in LT 3 has been maintained

at a constant level. The bar dissolved in this case as expected. On the other hand, to show that the evolution of halo prolateness is due to destabilizing action of the bar, we run models with a frozen axisymmetric disk in live triaxial halos — these models show basically no evolution for ϵ_H . We have also run a number of test models with the LT3 halo but smaller D/H mass ratio. Models with $D/H \lesssim 0.5$, formed only a weak oval distortion. This is unlike the trend in the axisymmetric live halos, where small D/H resulted in stronger bars. We discuss this below.

Second, the bar sizes appear to correlate with the halo core sizes, with the exception of live triaxial models where the bar size is more difficult to establish due to the strong response in the disk and a quick bar dissolution. The bar ellipticities provide additional source of information on the bar strength and even more about the state of the disk when the bar amplitudes measured by A_2 decay below 0.1.

Third, the pattern speeds of bars anticorrelate with halo core sizes — more centrally concentrated halos produce faster tumbling bars. However, the deceleration rate of the bar anticorrelates with the halo core sizes as well — thus, after the Hubble time, the end pattern speed of the bars is similar. As expected, bars in rigid halos quickly reach constant pattern speeds, while bars in live halos continue to slow down asymptotically. Interestingly, bars in live axisymmetric halos can become stronger or weaker while slowing down. Bars in live triaxial halos always weaken and dissolve while slowing down.

Fourth, in rigid halos, the angular momentum of the inner disk is fed into the outer disk, across the bar corotation. Some angular momentum is lost to the halo in rigid triaxial models. In live models, the halo appears to gain angular momentum, more so fractionally in triaxial models. We have verified that in axisymmetric models the angular momentum is mediated by lower resonances, especially by the inner Lindblad resonance in the disk and by the corotation resonance in the halo.

Finally, in triaxial models, as long as a bar is present, the disk evolution is characterized by development of a strong spiral structure outside the bar region. It is especially prominent in live triaxial halos. The outer disk acquires exponential surface density distribution, while the inner (bar-unstable) part can be modeled roughly by a shorter exponential scalelength when measured along the bar major axis.

Our emerging understanding of the evolution of bars embedded in live, mildly triaxial or axisymmetric halos is based on two physical processes which determine the fate of the system. These are the angular momentum redistribution in the disk-halo system and the development of chaos. We can make a general statement that angular momentum flows from the bar unstable region in the disk to the outer disk and the halo. This process is accompanied by the initial growth of the bar both in strength and in size. In axisymmetric halos, it ultimately saturates and the bar enters a steady-state phase characterized by secular changes (Athanasoula 2003). Instead, in a mildly triaxial halo which hosts a barred disk, the dominant process is the increase in the fraction of chaotic trajectories — it affects both the bar and halo structures. In other words, no steady-state devel-

ops, and either the bar is dissolved or halo prolateness is washed out. This effect on the bar embedded in a *rigid* triaxial halo has been calculated in ES02, and here we have presented fully self-consistent numerical simulations accounting for the bar and *live* halo evolution.

After the submission of this work we have learned about the work by Curir et al. (2005) where stellar disks have been evolved within the cosmological DM halos, albeit at much lower resolution than in our work. In these simulations, the bars form in response to the original torquing by the halo, but, contrary to our main results, survive for the rest of the simulation. We strongly suspect that this different behavior of bars results from the loss of prolateness by DM halos in their models, similarly to our model LT3. Furthermore, it is the process of introduction of disk into the halo which is also responsible for washing out the halo prolateness (Section 2.1), which required us to apply the second heating-cooling procedure. Unfortunately, Curir et al. do not provide any analysis of the shape of their halos after bringing up the disks and during their subsequent evolution. Their Table 1 refers to purely DM halos without stellar disks only.

Thus we expect that the combination of halo triaxiality and its cuspieness in conjunction with a fast rotating⁶ bar will lead to the development of chaos and to the dissolution of the least massive or structurally stable triaxial feature in the system, i.e., the bar or halo triaxiality. In section 1 (see also ES02 and refs. therein), we have argued that cuspy density distribution cause solutions for the Poisson equation to be far from quadratic and this will produce the coupling between different degrees of freedom in equations of motion which become highly nonlinear — a prime recipe to develop a chaotic behavior when such a system is perturbed.

To understand the results of these numerical simulations within the context of developing chaos in a triaxial system with a fast tumbling stellar bar, we take the next step and discuss the evolution of the bar strength in terms of the stability of trajectories used by ES02. Ultimately bars and other morphological features, such as prolate halos, dissolve when the density figure stops to support the figure of the background potential, in other words when self-consistency of density-potential pair is violated. As mentioned in section 1, a stable 3-D figure must be built from trajectories which at least approximately conserve the invariants of motion. Chaos appears when the number of invariants of motion becomes smaller than the dimensionality of the system.

Two issues appear most relevant in this respect: the overall asymmetry of the background potential and the degree of mass concentration. Stability of trajectories for potentials and density distributions used in this work have been analyzed in ES02 by calculating the Liapunov exponents on a high-resolution 3-D cylindrical grid. These exponents provide a measure of timescales which are associated with dynamical instabilities and are especially suitable to study development of chaotic motions in time-dependent potentials (see detailed description of this method in sections 1, 2 and the Appendix of ES02).

The mapping of halos which are under consideration

⁶ As defined in the footnote of section 1

here using the Liapunov exponents has shown that triaxial halos are regular in the absence of a bar — the top panel of Fig. 6 in ES02 indicates that trajectories within this potential are stable well over the Hubble time. This is supported by live models of triaxial halos presented here. All the models appear stable unless bar-unstable disks are added, *even the cuspy halo in LT 3*, as expected. It is the addition of a (triaxial) bar fast tumbling with respect to the halo, which destabilizes the trajectories and triggers the chaos. The middle panels in Fig. 6 of ES02 show this effect in a cuspy halo — most of the configuration space becomes chaotic with the characteristic timescale $\lesssim 1$ Gyr. Moreover, the chaotic regions are fully connected, thus providing a strong indication that survival of any non-axisymmetric structure is highly questionable. The less cuspy barred models of ES02 show progressively less chaotic regions, especially in the flat cores, and the existing chaos is less interconnected. A self-consistent bar-disk model of Pfenniger (1984), without a surrounding halo, shows chaotic regions confined to the bar corotation radius (lower panels, Fig. 6 of ES02), in line with the above explanation. We also note that the remarkable correspondence between the distributions of the available configuration space volume for the trajectories in ES02 and the maximal Liapunov exponents points out that the nearby stability islands are not efficient in trapping the chaotic trajectories. Therefore, one should expect that the predicted bar dissolution in ES02 models will indeed be observed in numerical simulations.

The sequences, RT 1→RT 3 and RT 1→RT 5 discussed in section 3 represent a gradual increase in the halo cuspi-ness, i.e., increased central mass concentration and progressively smaller size of the halo core. Figs. 3 and 6 of ES02 demonstrate that the regular (stable) region shrinks from $\sim 5 - 6$ kpc in RT 1 to about 0.5 kpc in RT 3, along with the increased halo cuspi-ness, not leaving much space for the bar to survive. When the bar feedback onto the halo is fully accounted for, i.e., in live triaxial halos — they also lose part of their asymmetry (prolateness) ϵ_H , but most of it remains. This explains why bars in LT 1 and LT 2 models behave qualitatively similarly to those in rigid RT models — all of them exhibit the bar dissolution.

The main difference between these models and the cuspy LT 3 is that cuspy halos are more structurally unstable, as we discussed above, and their prolateness is washed out early enough to allow for the bar to develop in a nearly axisymmetric environment. We confirm that either the onset of chaos dissolves the bar (e.g., LT 1 and LT 2) or it destroys the halo prolateness (e.g., LT 3). We strongly suspect that this latter process of is also at work in Curir et al. (2005) simulations of cosmological halos, allowing for long-lived bars. Therefore, to some extent long-lived bars are incompatible with the high (equatorial) asymmetry in the DM halos. Even the mild asymmetry observed in some halos of nearby galaxies is sufficient to shorten the bar lifetime to $\lesssim 5$ Gyrs.

This provides an interesting constraint on halo shapes, when taken in tandem with recent observational results. Using *HST*-based morphologies and accurate redshifts from the Galaxy Evolution from Morphology and SEDs (GEMS; Rix et al. 2004) survey, Jogee et al. (2004, hereafter J04; 2005) recently showed that the optical fraction and distribution of structural properties for bars

with moderate-to-high strength ($\epsilon \gtrsim 0.35$) remain similar from the present-day, out to look-back times of 2–8 Gyr ($z \sim 0.2 - 1.0$). J04 argue that these findings imply that on average bars have a long lifetime, well in excess of 2 Gyr. A constant optical bar fraction out to $z \sim 1$ is also reported independently from a smaller survey by Elmegreen et al. (2004). The simulations in this paper, when combined with these empirical results on a relatively constant fraction of bars out to $z \sim 1$ and an inferred long bar lifetime, put a lower limit on the halo equatorial axial ratio $\beta = b/a$ of 0.9 (in potential axes) at the redshift range of $z \sim 0 - 1$. This corresponds approximately to $(b/a)_\rho \sim 0.75 - 0.8$ axial ratio in *density* distribution.

The disappearance of triaxial halos with $\epsilon_H \gtrsim 0.1$ in disk galaxies at $z \lesssim 1$ seems as a corollary to our numerical simulations, when supplemented with the above observational results. As discussed in section 1, while cosmological simulations of dissipationless CDM galactic halos invariably produce triaxial halos, the triaxiality of the halo can be subsequently diluted by the addition of baryonic components. This is likely to happen, for instance, during the early formation and development of a galactic disk. Furthermore, this trend will be supported by a general decrease in the frequency of galaxy interactions and mergers below $z \sim 2$.

We note the following caveat: the halo prolateness in our modeled halos is (partially or fully) washed out by the action of the bar which leads to a dramatic increase in the fraction of chaotic orbits — these cannot support triaxial figures. It is the inner bar-forming part of the system where chaotic orbits dominate in asymmetric halos. In principle, we can envision the situation when the halo figure tumbles and trajectories which originate in its outer part cannot penetrate deep enough toward the central regions where they are typically destabilized. Such a halo will be more stable in preserving its prolateness, at least in its outer part. It is unclear how fast the halo must be tumbling for this effect to take place. Such models are beyond the scope of this work.

Finally, we find it important to address the question to what extent the evolution of stellar bars in our N -body potentials of mildly triaxial halos is *not* a numerical artifact, i.e., not a process driven by a numerical diffusion. In other words, can a Poisson noise, associated with the discreteness of the N -body potential, be primarily responsible for the observed model bar dissolution, as opposed to the chaotic behavior triggered by the competing forces from the triaxial halo and a bar in ES02 for smooth analytical potentials? One can argue that that the graininess of the N -body potential is identical in the axisymmetric and triaxial halo models. Because there is no indication that this potential has caused any numerical ‘relaxation’ effects in the former models, the latter ones will not be dominated by these effects as well. In principle, the consequences of the discreteness noise in the ‘mixed’ (triaxial halo/bar) models, i.e., models which are intrinsically more chaotic, can be more complex than in the axisymmetric models. Nevertheless, albeit indirectly, this supports our point of view that it is the chaotic dynamics which drives the evolution of stellar bar in triaxial halos modeled here.

To provide the most direct answer to this question is to analyze the numerical models presented here in terms

of Lyapunov exponents of ES02, but this is outside the scope of our work and will be addressed elsewhere. However, even if this approach will be taken, it is not without caveats as we deal here with a transient and not a classical chaos which is defined in the asymptotic limit and corresponds to an exponential divergence of a trajectory in a *fixed* potential (e.g., Lichtenberg & Lieberman 1995).

In summary, we find that even a mild halo triaxiality of ~ 0.9 in potential axial ratio, dissolves the stellar bar on a timescale of $\lesssim 5$ Gyr, sometimes leaving behind a weak oval distortion. Especially in the live triaxial halos, as long as a bar is present, strong spiral structure develop outside the bar and its strength depends on the mutual orientation of bars and the halo major axis. In comparable live axisymmetric halos, there is limited secular evolution, either growth or decay, of the embedded bars. In these cases, the halo core sizes correlate directly with the bar sizes and their central mass concentration — with the bar pattern speeds. Cuspy halos are more susceptible to washing out of their triaxiality due to the action of the bar, and the subsequent evolution is sim-

ilar to that of axisymmetric halos, where the bar does survive. We have interpreted the bar evolution in live asymmetric halos, as well as in mildly triaxial and cuspy models in terms of the orbital structure, the development of chaos and the feedback between the halo, disk and bar. We find that damping of the bar instability in such halos puts a tight upper limit on halo prolateness in *disk* galaxies in the range of redshifts extending from the local Universe to $z \sim 1$, in the light of recent results on a constant optical fraction of bar from the present-day out to these epochs.

We are grateful to Lia Athanassoula, Amr El-Zant, Clayton Heller and Inma Martinez-Valpuesta for numerous discussions. This research has been partially supported by NASA/LTSA grant NAG 5-13063 (S.J. and I.S.), NASA/ATP NAG 5-10823, HST AR-09546.01-A and 10284, and NSF grant AST-0206251 (I.S.). Simulations have been performed on a dedicated Linux Cluster and we thank Brian Doyle for technical support.

REFERENCES

- Aarseth, S.J., Binney, J. 1974, MNRAS, 185, 227
 Andersen, D.R., Bershady, M.A., Sparke, L.S., Gallagher, J.S. III, Wilcots, E.M. 2001, ApJ, 551, L131
 Athanassoula, E., Misiriotis, A. 2002, MNRAS, 330, 35
 Athanassoula, E. 2002, ApJ, 569, L83
 Athanassoula, E. 2003, MNRAS, 341, 1179
 Barnes, J.E., Efstathiou, G. 1987, ApJ, 319, 575
 Barnes, J., Hut, P. 1986, 324, 446
 Binney, J., Spergel, D. 1982, ApJ, 252, 308
 Binney, J., Tremaine, S. 1987, Galactic Dynamics, Princeton Univ. Press
 Borriello, A., Salucci, P. 2001, MNRAS, 323, 285
 Bullock, J.S. 2002, in The Shapes of Galaxies and Their Dark Halos, ed. P. Natarajan (Singapore: World Scientific), 109
 Burkert, A. 1995, ApJ, 447, L25
 Burkert, A.M., D’Onghia, E. 2004, astro-ph/0409540
 Buote, D.A., Canizares, C.R. 1994, ApJ, 427, 86
 Buote, D.A., Canizares, C.R. 1996, ApJ, 457, 177
 Buote, D.A., Jeltema, T.E., Canizares, C.R., Garmire, G.P. 2002, ApJ, 577, 183
 Christodoulou, D.M., Shlosman, I. & Tohline, J.E. 1995, ApJ, 443, 551
 Cole, S., Lacey, C. 1996, MNRAS, 281, 716
 Crone, M.M., Evrard, A.E., Richstone D.O. 1994, ApJ, 434, 402
 Curir, A., Mazzei, P., Murante, G. 2005, A&A, in press (astro-ph/0510182)
 de Blok, W.J.G., Bosma, A. 2002, A&A, 385, 816
 Dehnen, W. 2002, J. Comp. Phys., 179, 27
 Dekel, A., Shlosman, I. 1983, Internal Kinematics and Dynamics of Galaxies, ed. E. Athanassoula (Reidel Publ.), 187
 Dubinski, J., Carlberg, R.G. 1991, ApJ, 378, 496
 Dubinski, J. 1994, ApJ, 431, 617
 Elmegreen, B.G., Elmegreen, D.M., Hirst, A.C. 2004, ApJ, 612, 191
 El-Zant, A.A., Shlosman, I., Hoffman, Y. 2001, ApJ, 560, 636
 El-Zant, A.A., Shlosman, I. 2002, ApJ, 577, 626 (ES02)
 El-Zant, A.A., Shlosman, I., Begelman, M.C., Frank, J. 2003, ApJ, 590, 641
 El-Zant, A.A., Hoffman, Y., Primack, J., Combes, F., Shlosman, I. 2004, ApJ, 607, L75
 Flores, R.A., Primack, J.R. 1994, ApJ, 427, L1
 Frenk, C.S., White, S.D.M., Davis, M., Efstathiou, G. 1988, ApJ, 327, 507
 Friedli, D., Pfenniger, D. 1990, ESO/CTIO Workshop on Bulges of Galaxies, eds., B. Jarvis & D.M. Terndrup, p. 265
 Fukushige, T., Makino, J. 1997, ApJ, 477, L9
 Gentile, G., Salucci, P., Klein, U., Vergani, D., Kalberla, P. 2004, MNRAS, 351, 903
 Heller, C.H., Shlosman, I. 1994, ApJ, 424, 84
 Heller, C.H. 1995, ApJ, 455, 252
 Heller, C.H., Shlosman, I. 1996, ApJ, 471, 143
 Helmi, A. 2004, ApJ, 610, L97
 Hoekstra, H., Yee, H.K.C., Gladders, M.D. 2004, ApJ, 606, 67
 Holley-Bockelmann, K., Mihos, J.C., Sigurdsson, S., Hernquist, L. 2001, ApJ, 549, 862
 Huss, A., Jain, B., Steinmetz, M. 1999, ApJ, 517, 64
 Ideta, M., Hozumi, S. 2000, ApJ, 535, L91
 Jing, Y.P., Suto, Y. 2000, ApJ, 529, L69
 Jing, Y.P., Suto, Y. 2002, ApJ, 574, 538
 Jogee, S., Barazza, F.D., Rix, H.-W., Shlosman, I. et al. 2004, 615, L105 (J04)
 Jogee, S., et al. 2005, Penetrating Bars through Masks of Cosmic Dust, eds. D. Block, et al. (Dordrecht: Kluwer), in press (astro-ph/0408267)
 Kazantzidis, S., Kravtsov, A.V., Zentner, A.R., Allgood, B., Nagai, D., Moore, B. 2004, MNRAS, 354, 522
 Klypin, A., Kravtsov, A., Colin, P. 2000, Cosmic Flows Workshop, ASP Conf. Ser. 201, 344
 Kochanek, C.S. 1995, ApJ, 445, 559
 Kravtsov, A.V., Klypin, A.A., Bullock, J.S., Primack, J.R. 1998, ApJ, 502, 48
 Kuijken, K., Tremaine, S. 1994, ApJ, 421, 178
 Lichtenberg A.J., Lieberman M.A., 1995, Regular and Chaotic Dynamics. Springer, New York
 Lokas, E.L., Hoffman, Y. 2000, ApJ, 542, L139
 Martinez-Valpuesta, I., Shlosman, I. 2004, ApJ, 613, L29
 Martinez-Valpuesta, I., Shlosman, I., Heller, C.H. 2006, ApJ, 637, in press (astro-ph/0507219)
 McMillan, P.J., Dehnen, W. 2005, MNRAS, in press (astro-ph/0508647)
 Merrifield, M.R. 2002, Shapes of Galaxies and Their Dark Halos, ed. P. Natarajan (Singapore: World Scientific), 170
 Merritt, D., Valluri, M. 1996, ApJ, 471, 82
 Miyamoto, M., Nagai, R. 1975, PASJ, 27, 533
 Moore, B. 1994, Nature, 370, 629
 Moore, B., Quinn, T., Governato, F., Stadel, J., Lake, G. 1999, ApJ, 499, L5
 Moore, B., Kazantzidis, S., Diemand, J., Stadel, J. 2004, MNRAS, 354, 522
 Navarro, J.F., Frenk, C.S., White, S.D.M. 1996, ApJ, 462, 563 (NFW)
 Oguri, M., Lee, J., Suto, Y. 2003, ApJ, 599, 7
 Peng, E.W., Ford, H.C., Freeman, K.C. 2004, ApJ, 602, 685
 Pfenniger, D. 1984, A&A, 141, 171
 Pfenniger, D., Friedli, D. 1991, A&A, 252, 75
 Power, C., Navarro, J.F., Jenkins, A., Frenk, C.S., White, S.D.M., Springel, V., Stadel, J., Quinn, T. 2003, MNRAS, 338, 14
 Rix, H.-W., Zaritsky, D. 1995, ApJ, 447, 82
 Rix, H.-W. et al. 2004, ApJ Suppl., 152, 163

- Sackett, P.D., Rix, H.-W., Jarvis, B.J., Freeman, K.C. 1994, ApJ, 436, 629
- Sackett, P.D., Pogge, R.W. 1995, Dark Matter, eds. S.S. Holt & C.L. Bennett. AIP Conf. Proc., Vol. 336, p. 141 436, 629
- Sackett, P.D. 1999, Galaxy Dynamics, eds. D.R. Merritt, M. Valluri & J.A. Sellwood, ASP Conf. Ser. 182, 393
- Sand, D.J., Treu, T., Ellis, R.S. 2002, ApJ, 574, 129
- Sparke, L.S. 1986, MNRAS, 219, 657
- Tormen, G., Bouchet, F.R., White, S.D.M. 1997, MNRAS, 286, 865
- Warren, M.S., Quinn, P.J., Salmon, J.K., Zurek, W.H. 1992, ApJ, 399, 405
- Weinberg, M.D., Katz, N. 2002, ApJ, 580, 627